Coordination Chemistry Reviews 255 (2011) 790–803

Contents lists available at ScienceDirect

Coordination Chemistry Reviews

journal homepage: www.elsevier.com/locate/ccr

Review

Expanding the utility of proteins as platforms for coordination chemistry

Robert J. Radford, Jeffrey D. Brodin, Eric N. Salgado, F. Akif Tezcan*

Department of Chemistry and Biochemistry, University of California, San Diego, 9500 Gilman Dr., 6213 Urey Hall MC 0356, La Jolla, CA 92093-0356, USA

Contents

ARTICLE INFO

Article history:
Received 31 July 2010
Accepted 5 October 2010
Available online 14 October 2010

Keywords:
Bioinorganic chemistry
Metal–protein interactions
Self-assembly
Protein–protein interactions
X-ray crystallography
Protein design

ABSTRACT

Whether for constructing advanced materials and complex biological devices or for building sophisticated coordination complexes with diverse metal-based functions, proteins are nature's favorite building blocks. Yet, our ability to control the assembly of proteins or to use them as ligand platforms for inorganic chemistry has been somewhat limited. In this review, we highlight our work from the past four years, which has aimed to exploit the utility of a protein scaffold in both regards. First, by considering proteins as "simple" ligand platforms and controlling the metal coordination chemistry on their surfaces, we show how their self-assembly can be readily dictated by metal binding. Second, we show how metal-mediated protein self-assembly leads to novel metal centers buried within protein interfaces. While on one hand our studies have pointed out the challenges of using proteins as ligands, they have also revealed how the extensive, chemically-rich protein surfaces can be exploited to form a network of covalent and non-covalent interactions around interfacial metal centers, providing a powerful handle to control their coordination chemistry.

Abbreviations: bZIP, basic leucine zipper protein; CD, circular dichroism; Cyt cb_{562}, cytochrome cb_{562}; DFT, density functional theory; DMF, dimethylformamide; DMSO, dimethyl sulfoxide; EDTA, ethylene diamine tetraacetic acid; EGTA, ethylene glycol tetraacetic acid; FPLC, fast protein liquid chromatography; GuHCl, guanidine hydrochloride; HCM, hybrid coordination motif; HPhen, histidine:1,10-phenanthroline HCM; HQuin, histidine:8-hydroxyquinoline HCM; IA, iodoacetamide; ICP-OES, inductively coupled plasma optical emission spectroscopy; IDA, iminodiacetic acid; IMAC, immobilized metal affinity chromatography; K_d, equilibrium dissociation constant; MBP, metal binding protein; MBPC, metal binding protein complex; MeTIR, metal templated interface redesign; MOPS, 3-(N-morpholino)propanesulfonic acid; PPIs, protein–protein interactions; Phen, 1,10-phenanthroline; Quin, 8-hydroxyquinoline; RIDC, rosetta interface redesign complex; SASA, solvent accessible surface areas; Tris, tris(hydroxymethyl)aminomethane; VOC, vicinal oxygen chelate.

* Corresponding author. Tel.: +1 858 534 4862; fax: +1 858 534 6157.
E-mail address: tezcan@ucsd.edu (F.A. Tezcan).

0010-8545/$ – see front matter © 2010 Elsevier B.V. All rights reserved.
doi:10.1016/j.ccr.2010.10.010

1. Introduction

Proteins are particularly versatile ligands, not only because they feature a number of metal binding functionalities, but also because of their ability to form three-dimensional platforms that provide several layers of control over metal coordination and reactivity. It is thought that a large fraction of proteins are metalloproteins [1], which perform impressive tasks such as N_2 fixation, H_2O oxidation, CO_2 reduction, as well as selective functionalization of organic substrates [2]. Since these metal-centered activities are generally established once the metals are firmly placed within a protein scaffold, a great deal of attention has traditionally been paid to characterizing, mimicking and modifying such stable metal coordination sites in protein interiors [3,4]. Yet, recent advances in our understanding of cellular inorganic chemistry are indicating that the interactions of metals with protein surfaces are just as significant [5]. Metals or their complexes (e.g., metallodrugs) under physiological conditions are in constant contact with protein surfaces [6], which mediate their active transport to their cellular destinations [7], or which can crosslink proteins together leading to their aggregation [8]. Outside the cellular realm, metal–protein surface interactions form the basis of immobilized metal ion affinity chromatography (IMAC) [9], which has revolutionized protein biochemistry, as well as the functionalization of protein surfaces with metal complexes which have served as invaluable spectroscopic/functional probes [10,11] and catalytic sites [12,13].

Clearly, there is need and room for metal coordinating motifs that would enable a better control of inorganic chemistry on protein surfaces. Herein, we will review our recent efforts on expanding the use of coordination chemistry on the surfaces of proteins, allowing them to be literally used as metal ligands in a traditional, synthetic inorganic chemical sense. This approach has not only enabled the metal-guided engineering of discrete protein architectures with potential new utilities, but also provided a path to construct novel metal coordination sites within protein interfaces. What is more, this bottom–up approach has given us hints (or hypotheses) as to how nature may have evolved multiprotein complexes and functional metal centers. This work draws considerable inspiration from earlier works on fundamental inorganic coordination chemistry, supramolecular chemistry, and metalloprotein design/engineering where the interiors of already-formed metalloproteins or (semi)stable peptide assemblies have been creatively used for understanding bioinorganic design principles and for developing novel metal-based reactivities. These efforts in metalloprotein design have already been covered in excellent reviews by Pecoraro, Lu, DeGrado, Gibney, Barker [14–19] and many others. Some portions of this review were summarized in an earlier account [20]; although their inclusion here is necessary for the sake of completeness, greater emphasis will be given to our more recent work not covered in that account.

2. Coordination chemistry on protein surfaces

Our primary motivation to study the inorganic chemistry of protein surfaces stems from our desire to use metal coordination to control protein–protein interactions (PPIs) and protein self-assembly, which lie at the heart of nearly all cellular process and are predominantly responsible for the construction of biomachinery. The design and engineering of PPIs are plagued by the fact that they constitute extensive molecular surfaces made up of many weak interactions [21,22], which could in theory be replaced by a few appropriately engineered metal–ligand bonds. While this sounds straightforward to accomplish, this strategy is plagued by the chemical heterogeneity of protein surfaces (replete with carboxylates, amines, imidazoles, and thiol groups; Fig. 1(a)) that makes the site-selective localization of metals very challenging. To overcome this challenge, we decided to build chelating motifs on protein surfaces, just as a synthetic inorganic chemist would do in designing his/her ligand platforms.

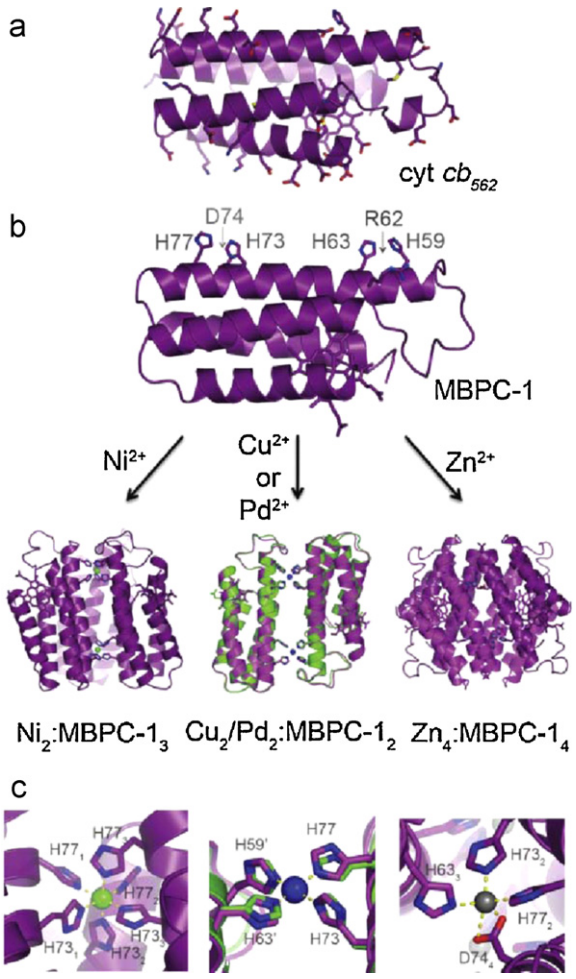

Fig. 1. (a) Cartoon representation of the four-helix-bundle hemeprotein, cytochrome cb_{562} (cyt cb_{562}). Amino acid side chains capable of coordinating metal ions are shown as sticks. (b) The cyt cb_{562} variant, MBPC-1, can self-assemble into discrete structures in a metal-dependent fashion based on the stereochemical preference of the added metal ion (a C_3 trimer with Ni^{2+}, a C_2 dimer with Cu^{2+} or Pd^{2+}, a D_2 tetramer with Zn^{2+}). (c) Close-up view of the interfacial metal centers in each metal-mediated complex.
Adapted from Ref. [20].

The α-helix is a particularly well-suited architecture for the installation of metal-chelating motifs, owing to the regular spacing of its amino acid constituents and its prevalence in the protein kingdom. In fact, nature frequently uses α-helices as scaffolds for metal chelation: amino acid residues (His, Glu, Asp) placed in $i/i+3$ and $i/i+4$ patterns (thus pointing in the same direction) are quite regularly used to construct bidentate metal binding sites, such as those in Zn-finger domains, and di-iron and di-copper centers to name a few [23]. Inspired by these natural examples, chemists have employed $i/i+3$ and $i/i+4$ bidentate motifs consisting of natural or unnatural metal ligands, with iminodiacetic acid (IDA) exemplifying the latter, to stabilize α-helical protein folds [24,25]; build de novo metalloproteins with stable mono- and dinuclear metal centers [23,26]; build substrate-selective metallopeptide catalysts [27]; and to facilitate purification by IMAC [28].

To explore the scope of coordination chemistry on protein surfaces, we chose the all-helical heme-protein cytochrome cb_{562} (cyt cb_{562}) as it is particularly stable [29], has a simple, cylindrical

shape (Fig. 1a), and is not prone to aggregation. As summarized below, several different surface chelating motifs were engineered on the cyt cb_{562} surface, which revealed some of the advantages and caveats of using individual proteins as ligands.

3. Exploiting natural chelates: coordination chemistry of surface *i*/*i*+4 bis-histidine motifs

The imidazole sidechain of His is an ideal component for a surface chelating motif, as its borderline soft imide nitrogen atoms possess a high affinity for most transition metals (relative to the carboxylates of the more common Asp and Glu residues) and it does not suffer from oxidation and covalent dimerization (as is common with Cys). When installed on an α-helical platform in an *i*/*i*+4 pattern, the bis-His motif provides metal dissociation constants that are in the low μM regime for late first-row transition metals (Co^{2+}, Ni^{2+}, Cu^{2+} and Zn^{2+}) [25,30]. In initial studies, two such bis-His motifs (His59/His63 and His73/His77) were incorporated near the ends of Helix3 of cyt cb_{562} to make the construct MBPC-1 (Fig. 1b), with the idea that metal coordination would lead to the oligomerization of this natively monomeric protein [31]. Indeed, the addition of equimolar Ni^{2+}, Cu^{2+} and Zn^{2+} to MBPC-1 results in the formation of discrete superprotein architectures that are commensurate with the stereochemical preferences of these metal ions (Fig. 1b and c): octahedral Ni^{2+} coordination promotes a C_3-symmetric trimer (Ni_2:MBPC-1_3) with the Ni's coordinated to three bis-His motifs donated by all three protomers; tetragonal Cu^{2+} produces a C_2-symmetric dimer (Cu_2:MBPC-1_2) with two bis-His motifs forming the equatorial coordination plane; and finally, tetrahedral Zn^{2+} coordination yields a D_2-symmetric tetramer (Zn_4:MBPC-1_4), where the Zn ligand set consists of a bis-His motif (H73/H77) from one protomer, a single His (H63) from a second, and an Asp (D74) from a third [31,32]. Ni^{2+}, Cu^{2+} and Zn^{2+} are all exchange labile ions that allow the metal-directed protein self-assembly to proceed under thermodynamic control. In the presence of Pd^{2+}, multiple oligomeric products are formed, as would be expected from the relative substitution inertness of this ion. Nevertheless, the predominant product is a dimer (Pd_2:MBPC-1_2) with an identical structure to Cu_2:MBPC-1_2, driven by the square-planar coordination of Pd^{2+} (Fig. 1c) [33].

These findings demonstrate that, in the absence of specific protein–protein interactions, the protein self-assembly is largely dictated by the stereochemical preference of the driving metal ion. Nevertheless, the coordination environment and the resulting supramolecular geometry of Zn_4:MBPC-1_4, for example, was in contrast to our expectations that a dimeric structure with Zn:His_4 coordination (one bis-His from each monomer) would be produced. Analytical ultracentrifugation studies revealed that a dimeric species indeed is formed at low Zn^{2+} and MBPC-1 concentrations, but it is subsequently replaced by the tetrameric architecture as the concentrations are increased [31].

4. The involvement of secondary interactions in metal-directed protein self-assembly

The crisscrossed Zn_4:MBPC-1_4 architecture results in extensive surface contacts among the protomers, with a total buried surface area of nearly 5000 Å^2 in the complex. To probe if these contacts have a collective influence on the thermodynamics of self-assembly without introducing extensive surface mutations, we instead made a small perturbation within the metal coordination sphere. Each Zn in Zn_4:MBPC-1_4 is coordinated by an Asp74 located within the 73/77 bis-His clamp in the *i*+1 position. Ligation by Asp74's is central to the observed supramolecular architecture of Zn_4:MBPC-1_4, in that they crosslink the MBPC-1 monomers at the Helix3

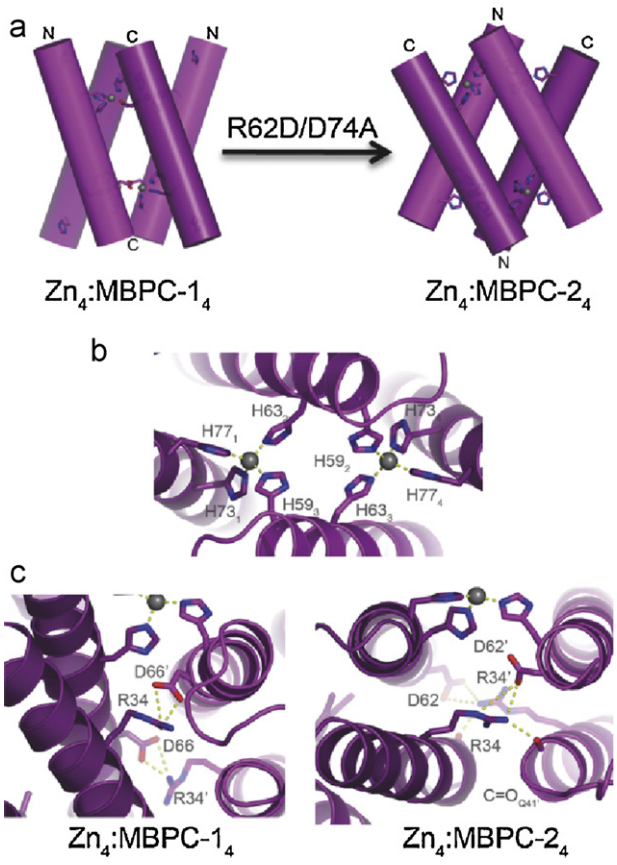

Fig. 2. (a) The conversion between the two Zn^{2+} mediated tetramers Zn_4:MBPC-1_4 and Zn_4:MBPC-2_4, shown in cylindrical cartoon representation. (b) Close-up view of interfacial metal centers in Zn_4:MBPC-2. (c) Key secondary interactions in the interfaces of Zn_4:MBPC-1_4 and Zn_4:MBPC-2_4.
Adapted from Ref. [34].

C-termini to yield the V-shaped dimers. If non-covalent interactions between protein monomers had negligible effect and metal coordination were the sole determinant of protein self-assembly, then the whole oligomeric assembly could be inverted by simply moving the coordinating Asp residue from within the C-terminal 73/77 bis-His clamp into the N-terminal 59/63 bis-His clamp motif at the *i*+3 position. Towards this end, we engineered MBPC-2, the R62D/D74A variant of MBPC-1 [34].

MBPC-2 forms a tetramer upon binding one molar equivalent of Zn according to analytical ultracentrifugation analyses. The crystal structure of Zn_4:MBPC-2_4 reveals a D_2-symmetrical architecture, which indeed is the "inverse" of Zn_4:MBPC-1_4 (Fig. 2a) [34]. Whereas the V shapes are joined at the Helix3 C-termini in the latter, they are crosslinked at the N-termini in the former. Unexpectedly, the newly engineered Asp62 is not involved in Zn binding. Instead, each Zn ion in the assembly is ligated by the 73/77 bis-His motif from one protomer, His59 from a second, and His63 from a third, again yielding a tetrahedral Zn coordination geometry. In this arrangement, coordination by His59 and His63 from two protomers – instead of the planned Asp62 and His63 coordination – stabilize the V's by splaying apart to bind two Zn ions and, in turn, joining the Helix3 N-termini (Fig. 2b).

Similarities between Zn_4:MBPC-1_4 and Zn_4:MBPC-2_4 structures suggest that tetrahedral Zn coordination again nucleates self-assembly and enforces D_2 supramolecular symmetry. Nevertheless, it is clear that metal coordination is not the only determinant of protein self-assembly, as MBPC-1 and MBPC-2 form distinctly different tetramers despite differing in only two residues situated far from the coordination sites. To probe the contribution of non-

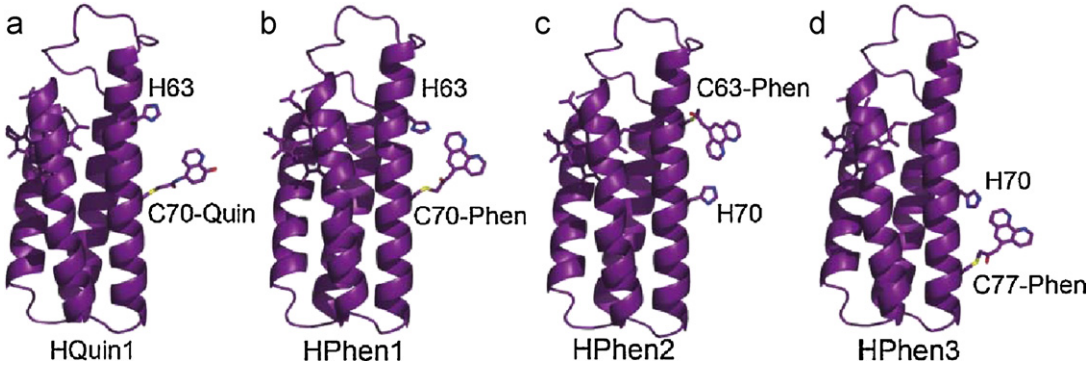

Fig. 3. Cartoon representation of cyt cb_{562} variants functionalized with hybrid coordination motifs (HCMs). Residues comprising the HCMs are shown as sticks. Adapted from Ref. [50].

covalent interactions in metal-directed self-assembly, we took a closer look at the interprotomeric interfaces in Zn_4:MBPC-1_4 and Zn_4:MBPC-2_4. This inspection revealed a set of salt–bridging interactions that stood out in each complex: between Arg34 and Asp66 in Zn_4:MBPC-1_4, and between Arg34 and Asp62 in Zn_4:MBPC-2_4 (Fig. 2c). Significantly, when these interactions are abolished through the Arg34Ala (MBPC-1) and Arg34Asp (MBPC-2) mutations, the tetrameric assemblies are replaced by heterogeneous ensembles that contain higher order aggregates [34]. These findings demonstrate that Arg34 interactions clearly are the guiding factor for the metal-induced oligomerization of MBPC-1 and 2.

The extent of the contribution of H-bonds and salt bridges to the stability of proteins and PPIs can vary from system to system [35–38]. Yet, these geometry-dependent interactions are important in limiting the number of possible low energy docking conformations, thus playing a major role in determining specificity [39,40]. Our findings indicate that salt–bridging and H-bonding interactions can dictate the geometric alignment of protein partners, leading to the population of discrete metal-directed supramolecular structures over other conformations of similar energy. Such sensitivity to secondary, non-covalent interactions makes our goal of predictably forming discrete superprotein architectures challenging, which we have attempted to circumvent through improved control of coordination chemistry on protein surfaces as described in the following section. At the same time, access to these secondary interactions may provide an additional handle to control metal-directed protein self-assembly, and importantly, to influence the coordination environment of the metal ions embedded in protein–protein interfaces. This possibility is described in Section 7.

5. Exploiting non-natural chelates – part 1: hybrid coordination motifs (HCMs) on protein surfaces

As outlined above, a big caveat to utilizing metal coordination to control protein self-assembly is the presence of numerous metal binding sidechain functionalities on any given protein surface, which bring about the challenge of controlling metal localization. Even when bidentate motifs like the $i/i+4$ bis-His pattern are employed, unexpected coordination arrangements that involve unforeseen amino acid functionalities can be observed as in the cases of Zn_4:MBPC-1_4 and Zn_4:MBPC-2_4. To exert more control over metal localization as well as metal-directed protein self-assembly, we sought to introduce non-natural chelating groups onto protein surfaces, which offer a far wider inorganic chemical spectrum than what is naturally available [41–43]. The use of non-natural chelating groups in metalloprotein engineering has recently been reviewed [13,14,44]. Non-natural groups like 1,10-phenanthroline [45,46], 2,2′-bipyridine [41,47], Schiff base complexes [48], and diphosphines [13] have been covalently incorporated into proteins using chemical modification of Cys residues, solid-phase synthesis, supramolecular anchoring or through in vivo/in vitro translation of non-natural amino acids. Among other uses, these metal chelates have been particularly useful for generating coordinatively unsaturated metal centers that, combined with the sterics of the surrounding protein environment, can perform selective chemical transformations.

We envisioned that bidentate chelates such as 1,10-phenanthroline (Phen) and 8-hydroxyquinoline (Quin) covalently linked to surface Cys's could be combined in an $i/i+7$ pattern – corresponding to a two-helix-turn separation – with a His on an α-helical surface to yield tridentate hybrid coordination motifs (HCMs). Such HCMs should not only provide improved metal affinities and selectivities, but also enable better control over protein oligomerization. Again using Helix3 of cyt cb_{562} as a platform, we constructed several Phen- and Quin-bearing HCM variants shown in Fig. 3 [49,50]. The Phen and Quin ligands were readily prepared in 60–75% yield as thiol-reactive iodoacetamide derivatives (IA-Phen and IA-Quin) using commercially available amino-precursors. Although IA-Phen and IA-Quin are sparingly soluble in water, they are easily introduced into cyt cb_{562} solutions after being solubilized in DMF or DMSO. Iodoacetamide functionalities have been extensively documented to rapidly and specifically modify Cys residues at near physiological pH [51]. Overall yields

Table 1
Dissociation constants, K_d, for Phen and Quin based HCM complexes compared to those for free 8-hydroxyquinoline (Quin) and 1,10-phenanthroline (Phen).

	Dissociation constants (M)						
	HQuin1[a]	AQuin1[a]	Free Quin[b]	HPhen1[a]	HPhen2[a]	HPhen3[a]	Free Phen[b]
Co^{2+}	$4.0\,(2)\times10^{-9}$	$3.0\,(1)\times10^{-7}$	6.5×10^{-7}	$3.3\,(2)\times10^{-10}$	$7.8\,(5)\times10^{-10}$	$2.0\,(2)\times10^{-9}$	8.0×10^{-8}
Ni^{2+}	$4.0\,(2)\times10^{-10}$	$3\,(1)\times10^{-8}$	1.5×10^{-7}	$7.8\,(6)\times10^{-10}$	$1.7\,(4)\times10^{-10}$	$1.6\,(3)\times10^{-10}$	3.9×10^{-8}
Cu2+	$8.5\,(9)\times10^{-14}$	$5.4\,(5)\times10^{-9}$	2.3×10^{-10}	$1.3\,(2)\times10^{-13}$	$1.2\,(2)\times10^{-13}$	$2.0\,(2)\times10^{-13}$	2.5×10^{-9}
Zn^{2+}	$7.1\,(3)\times10^{-9}$	$9\,(1)\times10^{-7}$	8.7×10^{-7}	$6\,(1)\times10^{-9}$	$3.8\,(3)\times10^{-9}$	$3.7\,(3)\times10^{-8}$	3.9×10^{-7}

[a] Dissociation constants determined by competition with EGTA in 50 mM MOPS (pH 7).
[b] pH-adjusted values based on reported K_d's [52]. (Adapted from Refs. [49,50].)

between 70 and 95% were routinely obtained for both the Phen and Quin labeled cyt cb_{562} variants.

5.1. Metal binding affinities of tridentate HCMs

An inherent advantage of HCMs is the spectroscopic handle that comes with most non-natural metal chelators. This feature allows the metal binding to be monitored spectroscopically without the need for extraneous reported ligands. Thus, the binding of Quin and Phen-HCMs to various divalent late-first-row transition metals (Co^{2+}, Ni^{2+}, Cu^{2+} and Zn^{2+}) were assessed by monitoring the π–π^* transitions of Quin (λ_{max} = 244 nm) and Phen (λ_{max} = 272 nm) that undergo 10–20 nm red-shifts upon metal coordination. The affinity of these tridentate HCMs for all of tested metal ions was too high (nanomolar or lower) to be reliably assessed by direct titrations; hence, ethylene glycol tetraacetic acid (EGTA) was used as a competing ligand to determine dissociation constants (K_d). As listed in Table 1, the tridentate nature of the Phen and Quin HCMs yield K_d's (nM–fM) that are at least three orders of magnitude lower than those of the $i/i+4$ bis-His motifs for each metal [49,50]. They are also considerably lower (by ~2 orders of magnitude) than those for free Phen and Quin ligands, which strongly suggests the participation of the His component of the HCMs in metal binding. Moreover, the affinities of HPhen1, 2 and 3 (which are equivalent in composition) for divalent metals are similar, and vary at most by six-fold, indicating that metal binding ability is not very sensitive to helix location or relative orientation of the HCM.

5.2. Metal-mediated α-helix stabilization through HCMs

In the process of binding metals with high affinity, $i/i+7$ HCMs also crosslinks a two-turn segment of Helix3, which could impart stability on this helix and thereby the entire protein. Previously, metal crosslinking of both natural and non-natural residues at $i/i+4$ positions has extensively been shown to induce α-helicity in peptides and significantly stabilize helical protein structures [25,30]. Likewise, covalent cross-linking of sidechain functionalities in $i/i+4$, $i/i+7$ or $i/i+11$ positions can lock small peptides in α-helical conformations [53–55], which in turn have proven to be promising pharmaceutical agents that effectively disrupt protein–protein interactions and exhibit increased resistance to proteases in vivo [56].

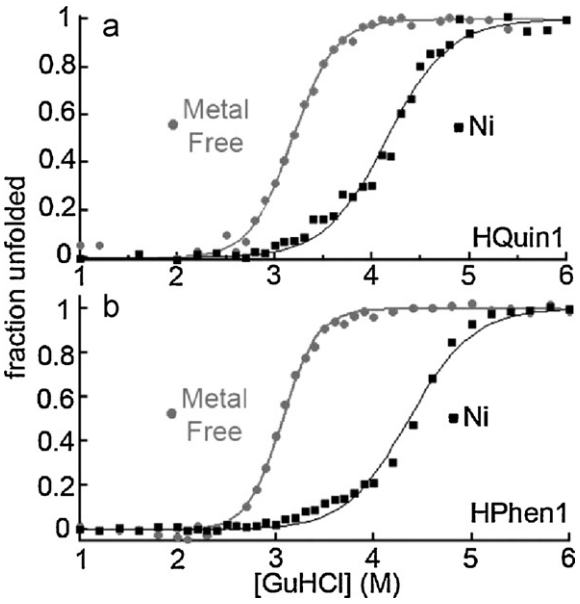

Fig. 4. Chemical unfolding of a 5 μM sample of (a) HQuin1 or (b) HPhen1 in 0.1 M Tris buffer pH 7. Unfolding titrations were performed in the presence (black squares) and absence (grey circles) of 1 mM Ni^{2+}, and monitored by CD spectroscopy. Adapted from Refs. [49,50].

In order to investigate the crosslinking ability of $i/i+7$ HCMs in the presence of metals, chemical (guanidine hydrochloride, GuHCl) unfolding studies were undertaken. The stability of all HQuin1 and all HPhen variants tested increased in the presence of divalent metal ions [49,50]. Fig. 4 shows representative unfolding titrations of the variants, each of which display a particularly enhanced stability in the presence of Ni^{2+}. We attribute the superior stabilizing effect of Ni^{2+} over other metals to the formation of an unstrained, facial coordination geometry by the His–Phen and His–Quin HCM, which was later crystallographically confirmed (see Fig. 7). Although it is tempting to link the thermodynamics of metal binding by the HCMs (Table 1) to that of metal-induced protein stabilization, such a correlation is complicated by the fact that net protein stabilization is a function of metal binding not only to the folded but also to the unfolded state, which may display multi-

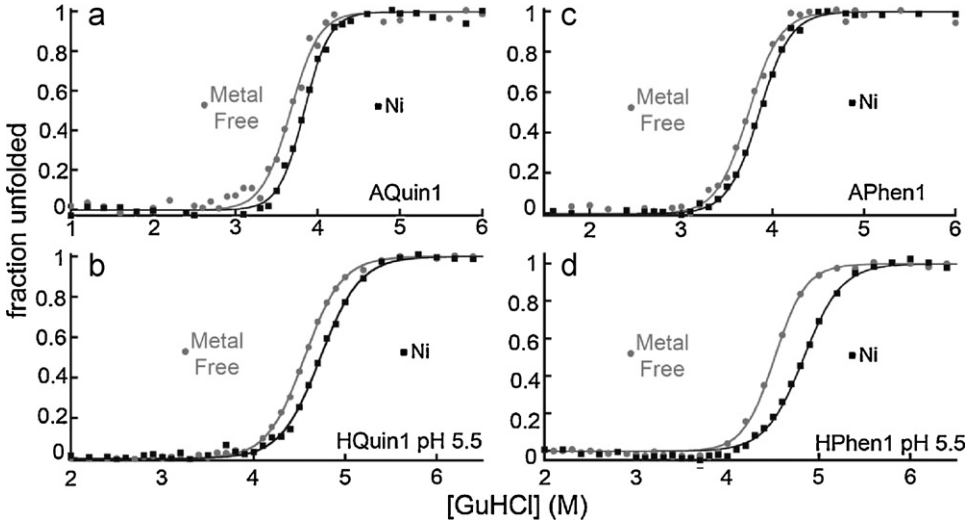

Fig. 5. Chemical unfolding of (a) AQuin1, (b) HQuin1 at pH 5.5, (c) APhen1 and (d) APhen1 at pH 5.5 in the presence (black squares) and absence (grey circles) of excess Ni^{2+}, as monitored by CD spectroscopy.
Adapted from Refs. [49,50].

ple modes of metal coordination, thus deviating from a two-state system [49]. The deviation from two-state behavior is evident in the shallower unfolding transitions of HQuin1 and HPhen1 in the presence of Ni^{2+} (Fig. 4).

The unfolding titrations for HPhen1 and HQuin1 were repeated at pH 5.5, where the His component would be protonated, or for variants which either lack the Phen and Quin ligand or have the His replaced by the noncoordinating residue Ala. The results indicate that, in all cases, Ni-induced stabilization is significantly diminished (Fig. 5), confirming the involvement of both His and Phen or Quin in metal coordination.

As mentioned above, stabilization of α-helical proteins and peptides by late-first-row transition metals is a well-established and utilized phenomenon. In one case, Gray, Arnold and co-workers instead utilized a substitution-inert capped Ru-complex ($Ru^{II}(bpy)_2CO_3$) to crosslink two His residues on two separate loops on the cytochrome *c* surface [57]. Whereas Cu^{2+} binding to these two His's led to a ~2 kcal/mol stabilization of the protein [58], the Ru-mediated crosslinking produced an impressive 5.5 kcal/mol increase in stability. This discrepancy can be attributed to the fact that the exchange-inert Ru^{2+} remains bound to the His's even in the unfolded state. Therefore, it not only enthalpically stabilizes the folded state, but also minimizes the entropy of folding through a preorganization of the unfolded protein. Motivated by these findings, we surmised that a capped, piano-stool Ru-complex can be accommodated by the facial, tridentate coordination geometry of the *i*/*i* + 7 His–Phen and His–Quin HCMs, and similarly lead to superior protein stabilization. One such Ru-complex, [dichloro(*p*-cymene) ruthenium (II) dimer], is commercially available (Fig. 6a), and weakly luminescent when bound to a polypyridines [59].

In a proof-of-principle study, a solution of HPhen1 was treated with 5-fold molar excess of compound Ru-*p*-cymene dimer dissolved in DMSO and reacted at room temperature for 4 days. Remarkably, the FPLC chromatogram and corresponding mass spectra revealed that the only species in solution is singly Ru-labeled HPhen1 [50], indicating that the His–Phen HCM provides a selective target for the Ru complex. As shown in Fig. 6c, Ru(*p*-cymene) adduct of HPhen1 is significantly more stabilized compared to the unmodified protein (or when it is in the presence of labile metal ions), with a corresponding free energy of stabilization

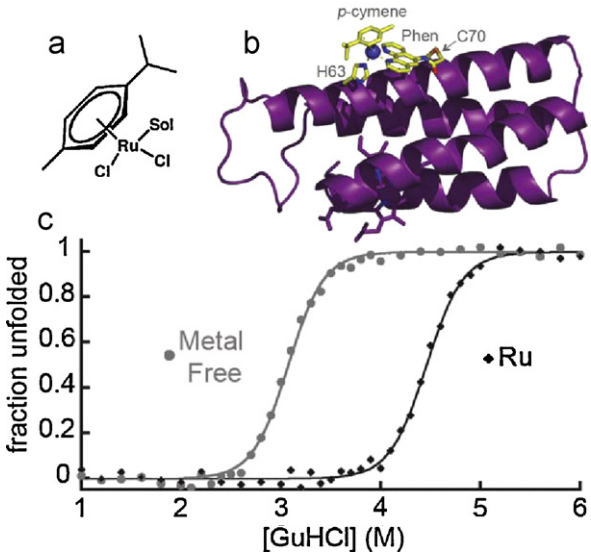

Fig. 6. Functionalization of HPhen1 with a substitution-inert Ru piano stool complex. (a) Solvated monomer of the commercially available dichloro(*p*-cymene)Ru(II) dimer. (b) A cartoon model of the proposed coordination for the Ru(*p*-cymene):HPhen1 adduct. (c) Chemical unfolding HPhen1 in the presence (black diamonds) and the absence (grey circles) of the Ru(*p*-cymene) group. Adapted from Ref. [50].

($\Delta\Delta G_{folding}$) by Ru(*p*-cymene) binding of 4.1 kcal/mol [50]. The fact that metal-mediated crosslinking of a local protein fragment leads to such protein stabilization is particularly significant given that the free energy of unfolding for natural proteins typically ranges from 5 to 15 kcal/mol [60]. This result also highlights the potential that HCMs may provide in selectively localizing metal-based probes.

5.3. Metal-mediated protein dimerization through HCMs

Upon establishing that *i*/*i* + 7 HCMs coordinate metals in the tridentate fashion as planned, we explored their utility in controlling protein–protein interactions (PPIs). The ability to control PPIs, both temporally and spatially, is an intensely pursued goal that is

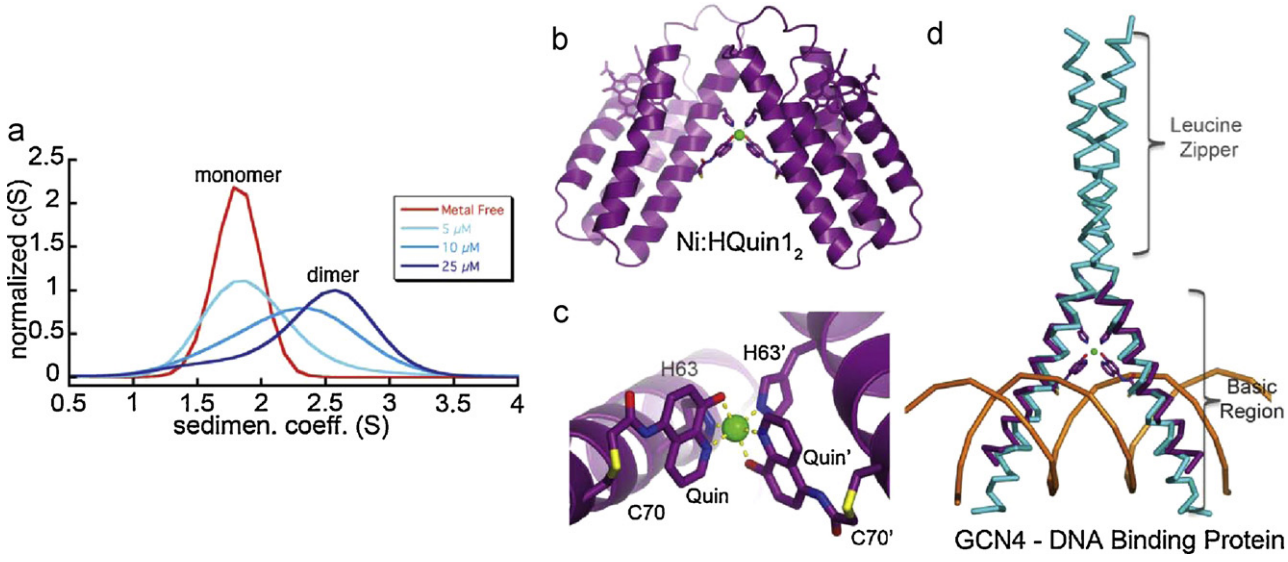

Fig. 7. (a) Sedimentation coefficient distributions for HQuin1 in the absence of metal and at various concentrations of HQuin1 with a half molar equivalent of Ni^{2+}. (b) Crystal structure of the Ni:HQuin1 dimer (PDB: 3L1 M). (c) A close-up view of the Ni^{2+} coordination environment in the Ni:HQuin1 dimer. (d) A superimposition of Helix3 from the Ni:HQuin1 dimer and the basic (DNA binding domain) of the transcription factor GCN4 (PDB: 1JNM). Adapted from Ref. [49].

complicated by the necessity to design extensive molecular surfaces [21,22]. Particularly challenging is to direct the self-assembly of proteins into discrete shapes that can recognize biological targets. This obstacle occurs at all levels of biomolecular recognition, including the case of homodimerization, which is the simplest and most prevalent form of protein self-assembly, extensively utilized throughout cellular signaling pathways [61]. We imagined that tridentate HCMs when available would promote efficient protein dimerization in response to an octahedral metal coordination geometry and impose a strict supramolecular geometry owing to their two-point attachment to the protein surface.

Sedimentation velocity (SV) experiments reveal that HPhen1 and HQuin1 readily dimerize in the presence of half an equivalent of Ni^{2+}, yielding a protein complex with a sedimentation coefficient of 2.6 S (Fig. 7a) [49,50]. The dissociation constants for the Ni:HPhen1_2 and Ni:HQuin1_2 dimers were determined by sedimentation equilibrium (SE) experiments to be ~9 μM and 42 μM, respectively [49,50]. Significantly, the dimeric stability of Ni:Phen1_2 and Ni:Quin1_2 closely approximate that of bZIP family transcription factors, which use peripheral leucine zippers domains for dimerization, with K_d's in the low micromolar range [62].

In order to understand the exact mode of Ni binding to His–Quin and His–Phen HCMs and Ni-induced dimerization, we obtained the crystal structure of the Ni:HQuin1_2 complex at 2.3 Å resolution (Fig. 7b) [49]. The asymmetric unit of the $P2_12_12$ crystals contains a single HQuin1 protomer coordinated to a half-occupied Ni^{2+} lying on a crystallographic two-fold symmetry axis. This two-fold symmetry produces a V-shaped dimer with a parallel arrangement of two HQuin1 protomers. The acute angle (~50°) between the protomers results in minimal contact (~300 $Å^2$ buried surface) between their surfaces and is entirely enforced by Ni coordination to His–Quin HCM's in a distorted octahedral geometry in Λ configuration. The Ni coordination sphere consists of a nearly ideal equatorial square plane formed by four nitrogen atoms from two H63's and Quin's, and two axial phenolate oxygen atoms that form a nonlinear O–Ni–O angle of 165° due in part to the small Quin bite angle of ~80° (Fig. 7c). The observed bond metrics closely approximate those of Ni^{2+} complexes with free quinolate and amine-type ligands [63]. This suggests that Ni coordination in the Ni:HQuin1_2 complex is free from steric constraints that may be imposed by the covalent attachment of the His–Quin HCM to the protein surface. Structural characterization of the Ni:HPhen1_2 dimer has remained elusive thus far. Nevertheless, based on the similarities between HPhen1 and HQuin1 and the fact that dimerization in both cases is entirely dictated by metal coordination, we can safely assume that the structure of Ni:HPhen1_2 would closely resemble that of the Ni:HQuin1_2.

A major objective of using metal coordination for directing protein self-assembly is to access biologically functional structures in a completely metal dependent, and easily predictable fashion. This goal would allow for the construction of biologically active structures with novel or expanded functionalities. We were excited to discover that structurally the V-shaped architecture of Ni:HQuin1_2 is closely reminiscent of the DNA-binding domains of the bZIP-family transcription factors. The bZIP proteins consist of a flexible, "proto-helical" basic domain that interacts with the DNA major groove and a helical leucine-zipper domain whose dimerization is necessary for the preorganization of the basic domain for stable DNA binding [64]. It has been shown in many instances that DNA recognition by bZIP proteins is sensitively dependent on the dimeric orientation of the basic domains [65,66]. A structural superposition of the Helix3 regions (M58-N80) of the Ni:HQuin1_2 dimer with the DNA-bound basic domain of a representative bZIP protein reveals a very close match, with a root-mean-square-deviation of 1.6 Å over 46 C_α's (Fig. 7d). This example demonstrates the potential utility of surface HCM's in directing the formation of rigid protein/peptide structures that are poised to recognize biological targets without the need for engineering extensive protein surfaces or peripheral oligomerization domains.

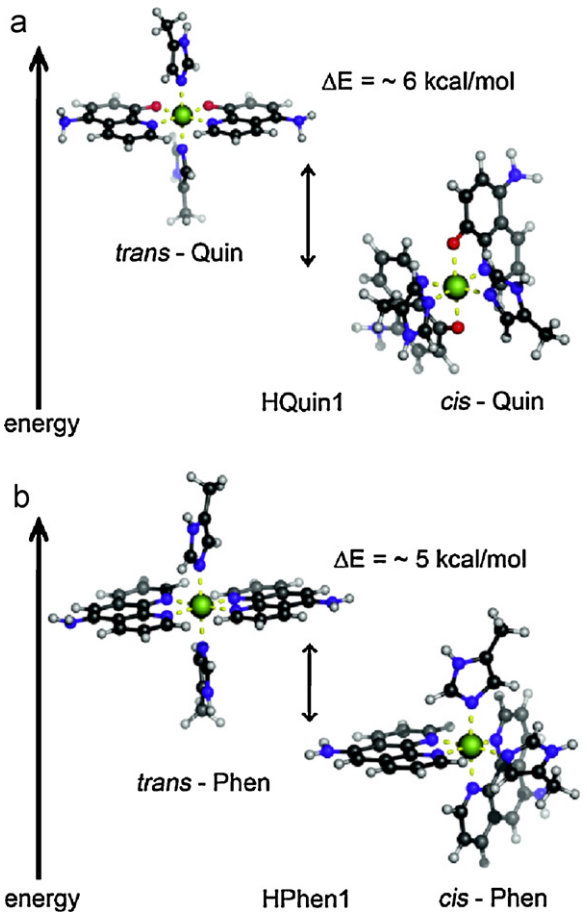

Fig. 8. Energy-minimized coordination geometries for the *cis* and *trans* isomers of (a) HQuin1 and (b) HPhen1.
Adapted from Refs. [49,50].

Stereochemical considerations suggest that there is one other possible isomer for His–Quin/Ni or His–Phen/Ni coordination that could lead to the formation of alternative HQuin1 and HPhen1 dimers in an antiparallel arrangement (Fig. 8). These alternative isomers would pose the Quin groups in a *trans* arrangement, whereby the equatorial plane would be formed by the Quin donor atoms and the axial positions would be occupied by the His ligands. In order to determine if there is a thermodynamic basis for the exclusive population of the observed "*cis*-Quin" and "*cis*-Phen" isomers, we performed density functional theory (DFT) calculations [49,50]. In both cases, the *cis* configuration was 5–6 kcal/mol more stable than *trans*, albeit due to different reasons. In the case of HQuin1 (Fig. 8a), the *trans* isomer is disfavored, because this arrangement would place the weaker-field phenolate oxygen atoms trans from the stronger imine ligands, which would be destabilizing. In the case of HPhen1 (Fig. 8b), where there is no distinction between the coordinating atoms from a ligand field perspective, it appears that there would be considerable steric clashes between the Phen hydrogen atoms that lie on the Ni equatorial plane, which would be relieved in the *cis*-Phen arrangement. No matter the underlying reason, the examples of both HQuin1 and HPhen1 demonstrate that dimerization of proteins can be programmed through a simple consideration of inner-sphere metal coordination, which is far more facile than designing extensive protein interfaces towards the same end.

6. Exploiting non-natural chelates – part 2: proteins as sterically bulky ligand platforms

One of the cornerstones of synthetic inorganic chemistry is the use of sterically bulky ligand platforms to secure a coordinatively unsaturated environment that is conducive to substrate binding and activation. In fact, proteins themselves are the "original" sterically bulky ligands that isolate their metal centers and often strain their inner-sphere coordination geometry to achieve reactivity, although such coordination chemistry takes place within the highly evolved and stable cores of metalloenzymes and proteins. Since in our approach, the metal coordinating surfaces of proteins become buried interfaces (i.e., pseudo-interiors) upon metal coordination, it may be possible to use the topological features of protein surfaces as steric encumbrance and construct coordinatively unsaturated metal centers.

6.1. Protein surface crevices as protective sites for metal coordination

One such topological feature on the cyt cb_{562} surface is the 40s/50s loop that unforeseeably created a protected binding pocket for Phen groups. The variant MBPPhen1 was constructed with a surface Phen attached to C59, in addition to H66 and H77, with the idea that H66 would complete an $i/i+7$ HCM with C59-Phen, and share metal coordination with H77 from another protein monomer (Fig. 9a) [67]. The crystal structure of the Ni^{2+} adduct of MBP-Phen1 instead revealed that rather than forming an HCM with H66, the Phen group is buried under an overhang formed by the 40s/50s loop (Fig. 9b). This placement of Phen protects the Ni ion from forming the expected $Ni(Phen)_3$ complex, and gives rise to the formation of an open trimeric architecture, Ni_3:MBPPhen1$_3$ (Fig. 9c), whose vertices are formed by three Ni ions, each coordinated to C59-Phen from one protein monomer, His77 from another and two solvent molecules (Fig. 9d) [67]. IR measurements on Ni_3:MBPPhen1$_3$ crystals indicate that the interfacial Ni centers can indeed accommodate extrinsic ligands like cyanate, which can replace the coordinating solvent molecules (Fig. 9e) [67].

In order to understand if there is a thermodynamic bias towards the burial of Phen under the 40s/50s loop and if this burial can yield alternative protein oligomers/frameworks with unsaturated metal centers, we constructed a variant of MBPPhen1 (MBPPhen2, Fig. 10a) that lacks H77 and H66. MBPPhen2 was crystallized in the presence of EDTA and its structure determined at 2.1 Å resolution [68]. The asymmetric unit of the C_2 symmetric lattice contains six MBPPhen2 monomers arranged in three pairs (Fig. 10b). Two of the pairs are identical to each other and feature a head-to-head alignment of monomers, where the Phen moieties form π-stacking interactions with one another while still buried under the 40s/50s loop (Fig. 10c). Significantly, the conformation of these 4 Phen groups in the asymmetric unit is identical to that observed in the Ni_3:MBPPhen1$_3$ (Fig. 9b): the aromatic moiety packs tightly into the cavity lined the side chains by T44, P53, M58, F61 and A62, and the amide nitrogen of the linker between C59 and Phen forms a H-bond with the backbone carbonyl of P53. The remaining pair of MBP-Phen2 molecules also forms a head-to-head dimer, but in contrast, their Phen groups are now observed outside of the surface crevice. One Phen group is pointing away from the 50s loop lying flat against the Helix3 surface (Fig. 10b), whereas the other one is significantly disordered as suggested by a weak corresponding electron density but still forming some π-stacking interactions with the former. While the crystal structure of metal-free MBPPhen2 indicates a preference of the Phen moiety to be buried under the 40s/50s loop, it also shows that it can explore other "out" conformations. To gain further insight into the energetics of Phen–protein surface interactions, we carried out alchemical free energy calculations, which indicate that the buried Phen conformation is 4.2 ± 1.3 kcal/mol more favorable than an extended and fully solvent-exposed conformation [68].

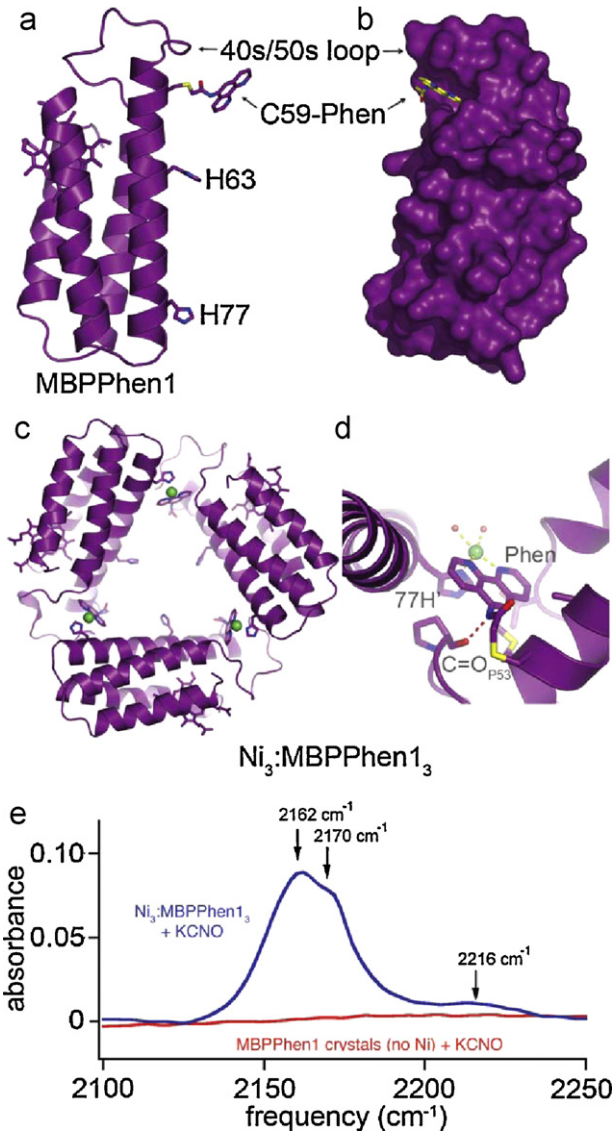

Fig. 9. (a) Cartoon representation of the cyt cb_{562} variant MBPPhen1, with key residues shown as sticks. (b) Surface representation highlighting the burial of the Phen moiety (yellow) within the 40s/50s loop crevice in the Ni_3:MBPPhen1$_3$ complex (PDB: 3FOO and 3FOP). (c) Supramolecular arrangement of the Ni_3:MBPPhen1$_3$ complex from the perspective of the 3-fold axis. (d) Close-up view of the Ni^{2+} coordination environment in the Ni_3:MBP-Phen1$_3$ with key interactions shown as sticks. (e) IR absorption spectra of Ni_3:MBPPhen1$_3$ crystals before and after exposure to potassium cyanate. (For interpretation of the references to color in this figure legend, the reader is referred to the web version of the article.)
Adapted from Ref. [67].

6.2. Protein oligomers and frameworks with coordinatively unsaturated metals sites

We next examined if the steric encumbrance around the Phen group in MBPPhen2 affects its coordination behavior. Specifically, we investigated the solution oligomerization state of MBPPhen2 in the presence of Ni^{2+}, which would be expected to give a trimeric species for a fully exposed Phen group. Sedimentation velocity (SV) experiments with MBPPhen2 in the presence of a 1/3 equivalent of Ni^{2+} to drive the formation of the Ni(MBPPhen2)$_3$ instead indicate

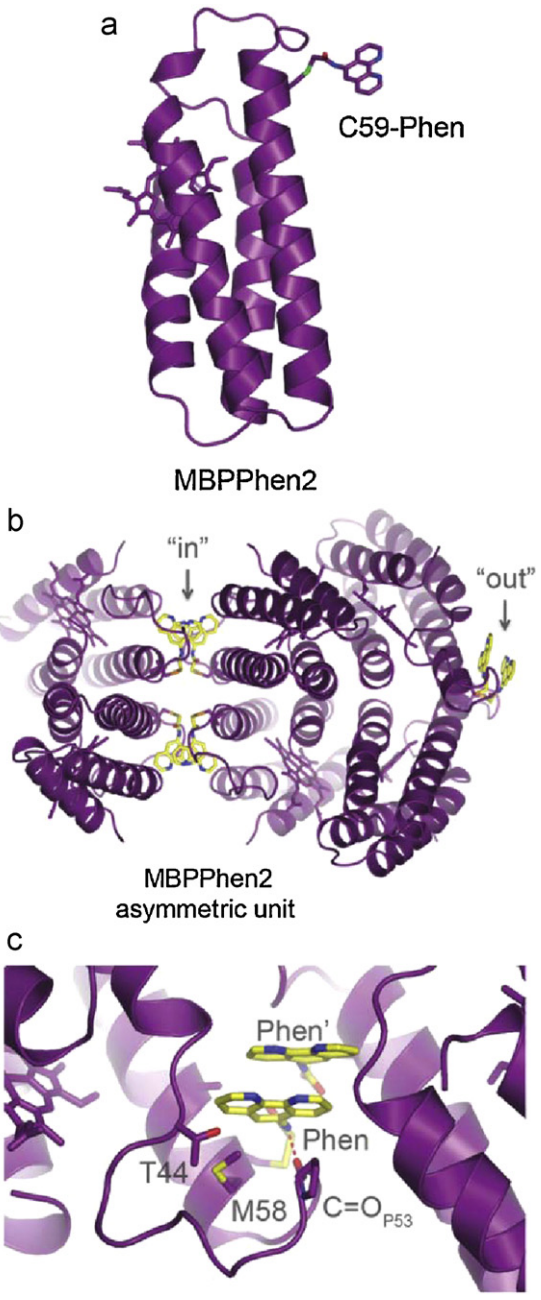

Fig. 10. (a) Cartoon representation of MBPPhen2 with the Phen moiety shown as sticks. (b) The contents of the asymmetric unit of metal-free MBPPhen2 crystals. (c) Close-up view of the "in" configuration, showing the π-stacking arrangement of neighboring Phen groups within the 40s/50s loop pocket. Key residues interacting with Phen groups are shown as sticks.
Adapted from ref. [68].

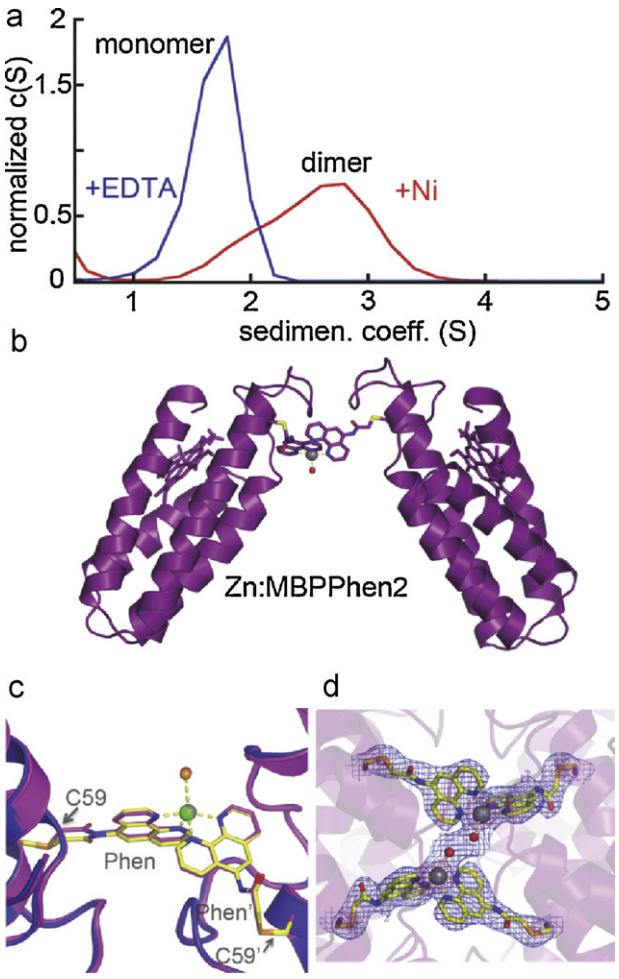

Fig. 11. (a) Sedimentation coefficient distribution for MBPPhen2 in the presence and absence of a 1/3 molar equivalent of Ni^{2+}. (b) Crystal structure of the Zn:MBPPhen2 dimer (PDB: 3MNK). (c) Superposition of Ni:MBPhen2 (yellow) and Zn:MBPPhen2 (magenta) metal centers. (d) Close-up view showing the proximity between the coordinatively unsaturated metal centers in the asymmetric unit of the Zn:MBPPhen2$_2$ structure. $2F_o - F_c$ electronic density map is contoured at 1.2 σ.
Adapted from Ref. [68].

that the predominant species in solution is a dimer (Fig. 11a), even at a protein/Ni concentration of 600/200 μM [68].

The solution oligomerization behavior of MBPPhen2 is paralleled in the solid state. We obtained crystals of the Ni^{2+} and Zn^{2+} adducts of MBPPhen2 and determined their structures at 3.1 and 2.8 Å resolution, respectively [68]. Remarkably, the hexagonal ($P6_5$ space group) crystals of the Ni^{2+} and Zn^{2+} complexes are entirely isostructural despite the distinct stereochemical preferences of the two ions. The Zn^{2+}-induced MBPPhen2 dimer is shown in Fig. 11b. This C_2-symmetric V-shaped dimer (or its Ni counterpart) is mediated solely by metal binding to Phen groups, one of which is in the buried and the other in an extended conformation. Ni and Zn are in identical distorted trigonal bipyramidal geometries, which are completed by a water molecule (Fig. 11c). In the asymmetric unit, pairs of Ni- and Zn-induced dimers are further interlaced, yielding D_2-symmetric tetramers that hold the metal centers in close proximity (7 Å between metal centers, 3 Å between coordinated water molecules, Fig. 11d). Clearly, the combination of the steric bulk around the Phen groups and lattice packing interactions are ultimately responsible for the formation of this particular supramolecular arrangement, and force Ni^{2+} and Zn^{2+} to adopt the same coordination geometry. The enforcement of identical coordination geometries on metal ions with distinct stereochemical preferences is typically reserved for rigid, bulky ligand platforms [69], which include highly evolved protein scaffolds with internal coordination sites. The fact that this can be achieved on the surface of a protein highlights the potential of crystalline protein frameworks being used as platforms for metal-based catalysis [70], as elegantly demonstrated in small-molecule crystal systems [71].

In support of such potential applications, crystals of the Ni^{2+} adducts of both MBPPhen1 and MBPPhen2 are highly porous. In the case of the former, the triangular Ni_3:MBPPhen1_3 oligomers stack up in the crystal lattice in an end-on-end fashion, which, due to the superposition of the four different trimer orientations, adopt an apparent hexagonal geometry (Fig. 12a). The resulting hexagonal

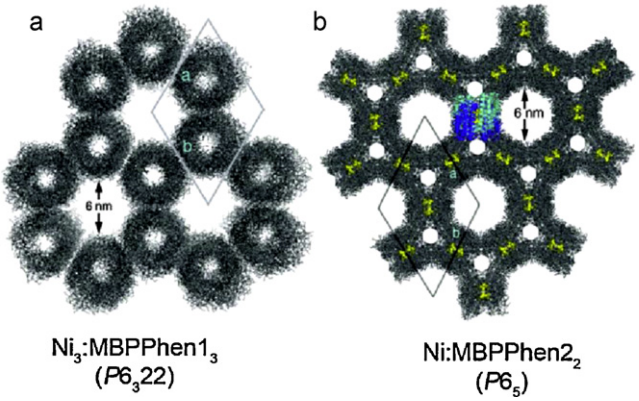

Fig. 12. Crystal lattices of the (a) Ni_3:MBPPhen1_3 (space group $P6_322$) and (b) Ni:MBPPhen2_2 ($P6_5$) complexes as viewed down the 6-fold symmetry axes. Adapted from Refs. [67,68].

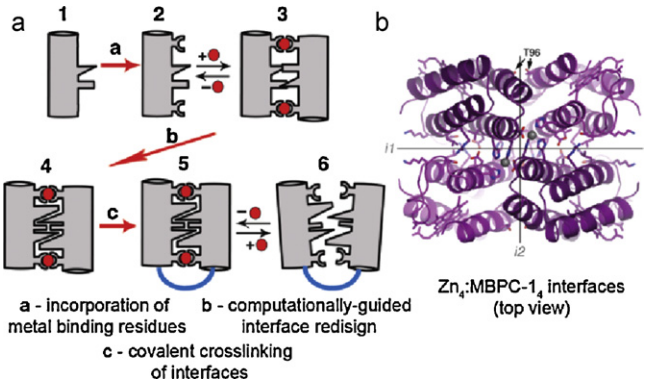

Fig. 13. (a) General scheme for metal-templated interface redesign (MeTIR). (b) Protein interfaces (*i1* and *i2)* in the D_2-symmetric Zn_4:MBPC-1_4 complex targeted for redesign. Key residues are shown as sticks. Adapted from Ref. [77].

tubes form a tightly-packed 2-D array with up to 64% solvent content. Likewise, Ni:MBPPhen2_2 dimers are arranged into columns using helix–helix packing interactions and form the lining of the two hexagonal channels, 6 and 2 nm wide, giving an overall solvent content of 61% (Fig. 12b). In both crystal forms, the interfacial metal centers appear to be accessible from the solvent channels, yet protected enough to potentially display selectivity.

As a prelude to reactivity studies, the Ni:MBPPhen2_2 crystals were subjected to chemical crosslinking with glutaraldehyde, which targets the amine groups of surface lysines. Whereas unmodified crystals immediately dissolve upon transfer from the precipitation solution (30% PEG400, 0.2 M ammonium sulfate) into water, the crosslinked crystals are indefinitely stable in water, even after being kept at 98 °C for 10 min, or in a 50% acetonitrile/water mixture. This further highlights the strong parallels between the metal complexes/frameworks (e.g., metal-organic frameworks) built with small organic ligands and those built with protein building blocks. While metal complexation by organic ligands is undoubtedly more predictable compared to that of proteins, and the resulting complexes more stable, proteins possess highly functional and functionalizable surfaces that provide additional handles to control coordination chemistry. This particular advantage of proteins as metal ligands is discussed in the following section.

7. Metal-templated ligand synthesis – with proteins

Inspired by nature, increasingly more sophisticated small ligand platforms are now being devised that incorporate non-covalent, outer-sphere interactions for the tuning of metal-centered reactivity [72,73]. Nevertheless, metalloproteins still provide control over the chemistry of metals to an extent that is difficult to match in such synthetic systems owing to the sheer number of covalent and non-covalent interactions in folded protein architectures that have been finely sculpted around metal centers by billions of years of evolution. Because the surface of a monomeric protein such as cyt cb_{562} is not evolved to function as part of an assembly, the interfaces in the complexes described above are not well packed and any advantage gained towards imparting metal specificity by using proteins as ligands is lost. To overcome this limitation, the large molecular surfaces (>1000 Å^2) between individual protein monomers in those complexes can be genetically engineered for complementarity to yield stable metalloprotein assemblies, and exploited to govern the chemistry of the embedded metal ions that templated the formation of the protein assemblies.

7.1. Metal-templated interface redesign

Starting with early work by Busch and coworkers [74], metal-templated synthesis has proven to be a powerful approach for constructing chelating and macrocylic ligands with enforced coordination geometries that provide stable and specific metal binding [74–76]. To demonstrate that this time-honored strategy can be extended to proteins, we developed metal-templated interface redesign (MeTIR), which is illustrated in Fig. 13a. Because Zn_4:MBPC-1_4 (Figs. 1b and 13b) possesses the largest of all protein interfaces (~5000 Å^2) that we have characterized, it was chosen as the initial system to demonstrate the feasibility of imparting metal specificity on a protein platform using MeTIR. The twofold dihedral symmetry of Zn_4:MBPC-1_4 presents three pairs of C_2-symmetric interfaces (*i*1, *i*2, *i*3) between its four protomeric constituents. Of these interfaces, the extensive buried surface (>1000 Å^2) and close protein–protein contacts of *i*1 make it the most ideal design target. We therefore undertook computationally-guided redesign of *i*1 to simulate the process of synthesizing a macrocyclic ligand around the Zn ion and generate a favorable set of interactions that would stabilize the entire Zn-driven assembly.

To achieve a successful redesign of interfaces, we developed a strategy that explicitly addressed (a) preserving the fold of the cyt cb_{562} monomer and (b) mutating the minimal number of residues that might have the maximal impact on protein–protein affinity within the Zn_4:MBPC-1_4 complex. For the first goal, we analyzed the structures and flagged as 'undesignable' all sequence positions in which the residues contacted the heme groups or Zn atoms (in Zn_4:MBPC-1_4), residues that had low solvent accessible surface areas (SASA), and residues that were involved in side chain-main chain H-bonds. For the second goal, the remaining set (designable residues) were subjected to rotamer optimizations using a variant of the RosettaDesign algorithms [78] used for optimizing multiple conformers for a single sequence [79]. In this case, each monomeric subunit of the tetramer represented a conformer. The designable residues were then ranked from high to low according to the Rosetta energy values and quality of packing (SASAprob) scores [80]. It was then determined which of those residues at the top of the list (i.e., poorly packed residues and residues with high energy) were at the interface. The neighboring residues of each non-optimal designable interface residue were then enumerated, which yielded clusters of designable residues. These clusters were subsequently used for redesign (i.e., concerted optimization of amino acid types at all cluster sequence positions).

Based on computational redesign of *i*1, we generated a construct, RIDC-1, which features six mostly hydrophilic-to-hydrophobic mutations (R34A/L38A/Q41W/K42S/D66W/V69I). As

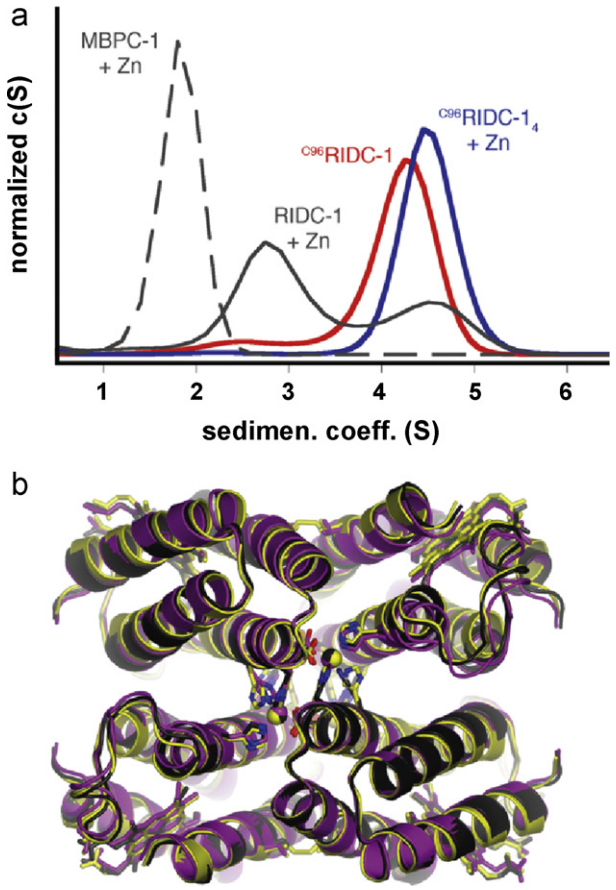

Fig. 14. (a) Sedimentation coefficient distributions for various cyt cb_{562} constructs (5 μM) in the presence of one equivalent of Zn^{2+}. (b) Structural superposition of the parent Zn_4:MBPC-1_4 complex with the redesigned Zn_4:^{C96}RIDC-1_4 assembly. Adapted from Ref. [77].

planned, this construct formed a considerably stabilized (Fig. 14a) tetrameric assembly (Zn_4:RIDC-1_4) with an identical supramolecular geometry to the parent tetramer (Fig. 14b) [81].

However, despite this stabilization, Zn_4:RIDC-1_4 (like Zn_4:MBPC-1_4) remained a dynamically exchanging assembly that did not stay intact, for instance, upon passage through a size-exclusion column. Consequently, it was not possible to uncouple protein oligomerization from Zn binding and directly assess whether interface redesign led to improvements in Zn affinity and selectivity. To overcome this limitation and obtain a stable tetrameric complex that would also form in the absence of Zn, RIDC-1 was further engineered.

The second stage of design was based on the dihedral symmetry of the Zn-tetramer, which dictates that the concurrent stabilization of any two of the three interfaces should, in principle, lead to the formation of a persistent tetrameric assembly. While interface *i*2 is not as tightly packed as *i*1 and therefore is less amenable to redesign, it presents position 96 (originally a threonine) from two protomers within an appropriate distance for disulfide (SS) crosslinking (Fig. 13b). We therefore surmised that *i*2 could be covalently stabilized by an interprotein disulfide bond (there are no other surface cysteines) and used along with the redesigned noncovalent interactions in *i*1 to create a stable, metal-independent tetrameric assembly. By combining the six mutations in *i*1 with the T96C mutation in *i*2, we generated a new construct, ^{C96}RIDC-1. Analytical ultracentrifugation experiments indicate that ^{C96}RIDC-1 forms a tetramer (^{C96}RIDC-1_4, $K_{d\text{-tetramer}} < 50$ nM) even in the absence of metal ions, providing a stable scaffold for investigation of our templating approach on metal affinity and selectivity [77].

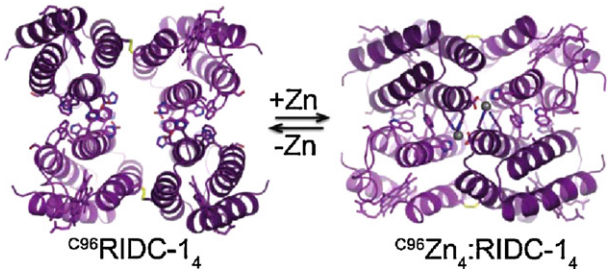

Fig. 15. Cartoon representation highlighting the conformational shift from ^{C96}RIDC-1 to Zn_4:^{C96}RIDC-1.
Adapted from Ref. [77].

7.2. Structural consequences of interface redesign

To understand the effects of our engineering efforts on the conformation of ^{C96}RIDC-1_4, we performed hydrodynamic measurements. Upon addition of Zn to ^{C96}RIDC-1_4, a shift in the sedimentation coefficient from 4.25 to 4.5 S (Fig. 14a) is observed, which suggests that the complex remains tetrameric upon Zn binding, but undergoes a large rearrangement. To elucidate this conformational change, crystal structures of ^{C96}RIDC-1_4 and its Zn adduct were determined at 2.1 and 2.4 Å resolution [77]. These structures reveal a remarkable scissor-like motion of the four protomers upon Zn-coordination, with a displacement of ~16 Å at the N-terminus of Helix3 (Fig. 15). In contrast to the completely covalent nature of most small molecule ligands, the simultaneous stability and conformational plasticity – hallmarks of many natural metallo-proteins – demonstrated by ^{C96}RIDC-1_4 is afforded by a combination of covalent and non-covalent interactions. The hydrophobic interactions built into *i*1 are stable, yet flexible enough to adopt multiple conformations. Simultaneously, the covalent SS bonds incorporated into *i*2 hold the protomers together (thus closing up the macrocycle), while still allowing them to undergo a significant translational and rotational motion relative to one another (Fig. 15). The resulting architecture of Zn_4:^{C96}RIDC-1_4 is superimposable onto both Zn_4:MBPC-1_4 and Zn_4:RIDC-1_4 structures with respective root-mean-square deviations of 0.59 and 0.63 Å over 424 C_α's (Fig. 14b). Importantly, the coordination environment of the four Zn ions (formed by H63/H73/H77/D74) is maintained after the interfacial modifications, as intended by the "template-and-stabilize" approach.

7.3. Functional consequences of interface redesign – evolution of metal binding stability and selectivity

With protein oligomerization now uncoupled from metal binding, we examined if our interface templating strategy indeed provided increased Zn affinity and selectivity through competitive metal binding titrations. These titrations indicated the binding of four equivalents of Zn to ^{C96}RIDC-1_4, as expected, with an average dissociation constant in the low nM regime (Table 2) [77]. Given that $i/i+4$ bis-His motifs (present on the parent protein construct MBPC-1) on α-helices display Zn dissociation constants in the low μM range [30], the Zn binding titrations suggest that the pre-formation of a tetrameric, templated acceptor complex results in a ≥1000-fold increase in Zn-binding affinity relative to the monomeric parent species, MBPC-1.

To elucidate if MeTIR also leads to Zn selectivity, we examined the interactions of ^{C96}RIDC-1_4 with several other divalent metal ions (M^{2+}), including the neighboring Co^{2+}, Ni^{2+} and Cu^{2+} [77].

Table 2
Dissociation constants for various metal binding equilibrium models for ^{C96}RIDC-1_4 determined through competitive fura-titrations (pH 7, 295 K)[a].

Total metal equivalents	Number of consecutive binding equilibria	K_d1 (M)	K_d2 (M)	K_d3 (M)	K_d4 (M)	Total $-\Delta G$ for metal binding (kJ mol^{-1})
$4Zn^{2+}$	2	$5.2(4)\times10^{-10}$	$4.3(2)\times10^{-8}$			189
	4	$1.3(3)\times10^{-9}$	$5.3(7)\times10^{-10}$	$3.3(8)\times10^{-8}$	$5.8(8)\times10^{-8}$	186
$2Cu^{2+}$	1	$1.0(1)\times10^{-12}$				136
	2	$2.5(3)\times10^{-13}$	$1.4(1)\times10^{-12}$			138
$2Ni^{2+}$	1	$8.0(9)\times10^{-9}$				92
	2	$9.0(1)\times10^{-10}$	$4.9(5)\times10^{-9}$			93
$1Co^{2+}$	1	$9(4)\times10^{-7}$				34

[a] The total free energies for metal binding correspond to the free energy sums of individual equilibria (times their multiplicity) for every model. Numbers in parentheses correspond to standard deviation in the last reported significant figure, were obtained through DynaFit, and do not include any experimental errors. (Adapted from Ref. [77].)

Competition studies, summarized in Fig. 16, revealed that ^{C96}RIDC-1_4 does in fact display significant Zn selectivity over all tested metal ions except Cu^{2+}, completely outcompeting Co^{2+} at all ratios measured (up to 100 Co:1 Zn), and exhibiting an effective affinity roughly 100-fold higher than Ni^{2+}. In contrast, previous studies have shown the affinity of the $i/i+4$ bis-His motif (our starting metal binding motif before templated interface redesign) for Zn^{2+} to be comparable to that for Ni^{2+} and 5–10 fold higher than that for Co^{2+} [25,30]. Taken together, these results indicate that our templating strategy indeed imparts a significance preference for tetrahedral Zn coordination.

Cu^{2+} presents a special case in terms of Zn selectivity. Due to a combination of its d^9 configuration and high Lewis acidity, Cu^{2+} is situated at the top of the Irving–Williams series, leading to its higher affinity for most ligand platforms designed for specific Zn binding [82,83] and even natural Zn enzymes [84]. Initial results shown in Fig. 16 indicated that neither Cu^{2+} nor Zn^{2+} outcompete each other for ^{C96}RIDC-1_4 binding. Rather, each tetrameric ^{C96}RIDC-1_4 unit appeared to bind ~3 equivalents of each ion in the non-coordinating MOPS buffer solution. To ascertain whether this apparent oversaturation of ^{C96}RIDC-1_4 is due to the binding of Cu^{2+} or Zn^{2+} ions to the ^{C96}RIDC-1_4 surface, we obtained crystals of ^{C96}RIDC-1_4 grown in the presence of equimolar amounts of both ions. The resulting 2.1 Å resolution diffraction data reveal a structure identical to that of Zn_4:^{C96}RIDC-1_4. Anomalous difference maps calculated from data sets collected at the Zn and Cu K absorption edges (Fig. 17a and b) unambiguously indicate the presence of Zn and not Cu at core metal binding sites. Given that both metals are present in the crystal as clearly indicated by X-ray fluorescence measurements (Fig. 17c), we conclude that Cu^{2+} ions are weakly bound to a large number of partially occupied surface sites.

In addition, when the Zn–Cu competition experiments are carried out in a coordinating buffer solution (20 mM TRIS) as opposed to the noncoordinating MOPS buffer, the amount of Cu^{2+} associated with ^{C96}RIDC-1_4 is significantly diminished, whereas the amount of bound Zn^{2+} stays constant (Fig. 16). These observations suggest that our design efforts resulted in a ligand platform, in which Zn^{2+} completely outcompetes Cu^{2+} for binding to the core sites, a feat rarely accomplished in designed protein or small molecule systems.

To describe the Zn selectivity of ^{C96}RIDC-1_4 in a more quantitative fashion, we examined its affinity for Co^{2+}, Ni^{2+} and Cu^{2+}. Titrations with these ions indicate that ^{C96}RIDC-1_4 has one weak Co^{2+} binding site, and that it can accommodate two equivalents of Ni^{2+} or Cu^{2+} with affinities that are either similar to those for Zn^{2+} (in the case of Ni^{2+}) or 2–3 orders of magnitude higher (in the case of Cu^{2+}) (Table 2). However, the higher multiplicity for Zn^{2+} binding (4 equivalents) apparently results in a considerably more favorable overall free energy (~190 kJ/mol compared to 140 kJ/mol for Cu^{2+} and 90 kJ/mol for Ni^{2+}), and ultimately in the Zn selectivity of ^{C96}RIDC-1_4 over these ions. Thus, templated interface redesign leads to increased bias not only towards Zn coordination geometry

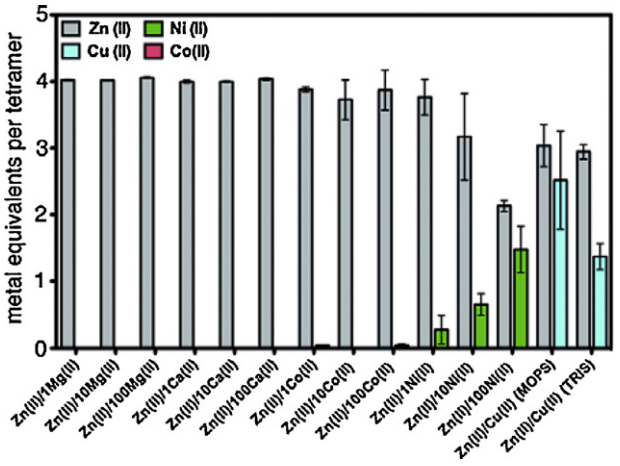

Fig. 16. Extent of divalent metal ion binding to ^{C96}RIDC-1_4 in competition experiments as determined by ICP-OES.
Adapted from Ref. [77].

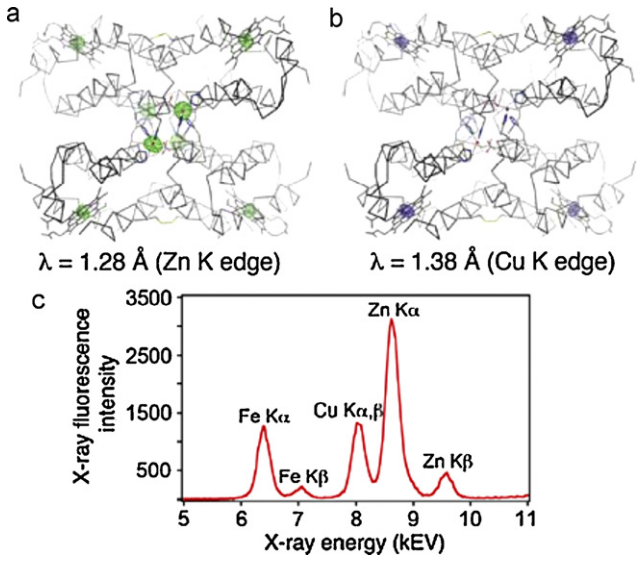

Fig. 17. Anomalous difference maps (contoured at 4σ) for ^{C96}RIDC-1_4 crystals grown in the presence of equimolar Cu^{2+} and Zn^{2+}, which were obtained at the Zn (a) or Cu (b) K edges. The heme Fe centers show anomalous signals at both wavelengths, whereas the core metal sites do the same only at the higher energy Zn edge, unambiguously identifying them as Zn ions. (c) X-ray fluorescence excitation scans of the same crystal indicate the presence of both Zn and Cu.
Adapted from Ref. [77].

but also towards Zn binding multiplicity, which, to our knowledge, is a rare, and perhaps unique, case in designed/synthetic systems.

7.4. Evolutionary implications of metal-templated interface redesign

The incorporation of metal ions into correct biological targets is central to cellular functioning and often necessitates non-trivial strategies such as the control of absolute and relative ambient metal concentrations [85], active delivery via chaperones [86], and compartmentalization [87]. All of these strategies still require the target protein to possess an intrinsic affinity and selectivity for the desired metal ion. Nevertheless, how protein structures originally evolved to stably and selectively bind metal ions and developed metal-dependent functions is not immediately evident from genomic and proteomic analyses. Some contemporary metalloproteins likely were based on pre-existing protein folds that acquired the ability to bind metals through random genetic events and subsequently attained their current structures and functions in the course of natural selection [88]. Alternatively, metal ions could first have templated the formation of a protein/peptide aggregate, followed by the evolution of the protein structure around the metal ion [89], as we have attempted to emulate with MeTIR.

Based on structural analysis, Hol and co-worker proposed that all α-helical dioxygen transport proteins such as hemocyanin and hemerythrin (and even hemoglobin) could have arisen from a common ancestor ("a primordial metal-binding helical pair"), which was produced by the metal-mediated dimerization of helical domains [90]. This symmetrical metallodimer later was subjected to multiple gene fusion and duplication events to ultimately yield the modern protein products that display a pseudo C_2 symmetry around their di-copper and di-iron centers. Armstrong, in his analysis of the diverse metalloprotein family of vicinal oxygen chelates (VOCs), also suggested a similar evolutionary pathway based on a metal-dimerized common ancestor [91]. The VOC superfamily is composed of structurally related proteins with paired βαβββ motifs that can house an array of divalent metal ions (Mg^{2+}, Mn^{2+}, Fe^{2+}, Co^{2+}, Ni^{2+}, Zn^{2+}). This particular fold leads to two to three open coordination sites on the metal centers to enable their direct participation in isomerization, epimerization, oxidative cleavage and nucleophilic substitution reactions. It was proposed by Armstrong [91] – and earlier by Bolin and co-workers [92] – that the VOC superfamily also originally evolved from a metal-directed C_2 symmetrical dimer of βαβββ motifs, which underwent gene duplication, fusion, modification and domain swapping events to generate the diverse superfamily. It is easy to envision how different metal ions could be swapped for one another within these multi-βαβββ scaffolds once sufficient structural rigidity was achieved during evolution. Indeed, some VOCs function just as well when their active sites are substituted with alternative metal ions [91].

While evolution cannot be proven, our results provide an experimental demonstration for the feasibility of an evolutionary pathway initiated by a metal-directed oligomerization event, such as those hypothesized by Hol, Bolin and Armstrong. Namely, a helical scaffold (cyt cb_{562}) is transformed into a Zn-selective/responsive tetrameric complex through an initial metal-mediated nucleation step. The resulting complex is then evolved into a functional assembly (the function being Zn selectivity) by stepwise mutations, which correspond to less that 10% of the amino acid sequence of cyt cb_{562} and each of which (hydrophobic mutations to stabilize protein interfaces, surface Cys mutations to crosslink multiple domains together around the metals) had a positive functional consequence towards the Zn-selectivity as is the case for natural selection.

A hallmark of evolution is not only the creation of a specific, beneficial function through a succession of random events, but also the creation of functional diversity, which increases the likelihood of survival for an evolving species. Tawfik and co-worker have championed the view that functional diversity would be best achieved through flexible protein structures/evolutionary intermediates that can accommodate different substrates (or metal ions) [93], around which the rigid protein architectures can then evolve for specific functions. In our case, the structural plasticity of the ^{C96}RIDC-1_4 architecture allows binding of various metal ions in its core, despite being highly Zn-selective, and imparts the ability to adopt different supramolecular and metal-coordination geometries. Current work in our lab aims to probe through rational mutagenesis and directed evolution strategies whether higher metal-based functions, such as redox reactivity and catalysis can emerge from such flexible, metal-templated superprotein architectures.

8. Conclusions

Here we have summarized our work over the last four years on establishing proteins as "new" ligand platforms for coordination chemistry. Although nature has been using proteins as metal platforms for billions of years, and chemists have exploited the interiors of stable proteins and peptide assemblies to the same end, proteins had not been considered as building blocks for inorganic chemistry in the traditional sense. We have shown that proteins can indeed be treated as such: with the appropriate placement of metal-binding sidechain functionalities on the surface, they form complexes dictated by the stereochemical preferences of the metal ions. They can be exploited as sterically bulky ligands to create coordinatively unsaturated metal centers within interfaces. They can be arranged into ordered metal-driven frameworks just like their small organic counterparts. All this comes with the caveat that metal coordination on protein surfaces is not nearly as predictable as with synthetic ligands because of the chemical heterogeneity of the former. Nevertheless, this chemical heterogeneity also translates into powerful handles – i.e., extensive non-covalent and covalent interactions – to control coordination chemistry, which makes us very excited about the potential of proteins as novel ligand platforms.

Acknowledgments

This review is dedicated to Prof. Harry Gray, who continues to be a source of inspiration and target of aspiration. We thank the members of the Tezcan Group and UCSD Inorganic Chemistry faculty for many helpful discussions, Prof. Arnie Rheingold for his crystallographic expertise, and acknowledge the following agencies for financial support of the work discussed here: NSF (CHE-0908115), DOE BES (DE-FG02-10ER46677), the Arnold and Mabel Beckman Foundation, the Sloan Foundation, the Hellman Family Fund, and UCSD.

References

[1] K.J. Waldron, N.J. Robinson, Nat. Rev. Microbiol. 7 (2009) 25.
[2] I. Bertini, H.B. Gray, E.I. Stiefel, J.S. Valentine, Biological Inorganic Chemistry, Structure & Reactivity, University Science Books, Sausalito, 2007.
[3] R.H. Holm, E.I. Solomon, Chem. Rev. 104 (2004) 347.
[4] Y. Lu, S.M. Berry, T.D. Pfister, Chem. Rev. 101 (2001) 3047.
[5] A.E. Palmer, K.J. Franz, Chem. Rev. 109 (2009) 4533.
[6] A.V. Klein, T.W. Hambley, Chem. Rev. 109 (2009) 4911.
[7] A.K. Boal, A.C. Rosenzweig, Chem. Rev. 109 (2009) 4760.
[8] W. Maret, Y. Li, Chem. Rev. 109 (2009) 4682.
[9] F.H. Arnold, B.L. Haymore, Science 252 (1991) 1796.
[10] J.R. Winkler, H.B. Gray, Chem. Rev. 92 (1992) 369.
[11] S.R. Adams, R.E. Campbell, L.A. Gross, B.R. Martin, G.K. Walkup, Y. Yao, J. Llopis, R.Y. Tsien, J. Am. Chem. Soc. 124 (2002) 6063.
[12] J. Podtetenieff, A. Taglieber, E. Bill, E.J. Reijerse, M.T. Reetz, Angew. Chem. Int. Ed. 49 (2010) 5151.
[13] T. Heinisch, T.R. Ward, Curr. Opin. Chem. Biol. 14 (2010) 184.
[14] Y. Lu, N. Yeung, N. Sieracki, N.M. Marshall, Nature 460 (2009) 855.
[15] D. Ghosh, V.L. Pecoraro, Curr. Opin. Chem. Biol. 9 (2005) 97.

[16] M.A. Case, G.L. McLendon, Acc. Chem. Res. 37 (2004) 754.
[17] P.D. Barker, Curr. Opin. Struct. Biol. 13 (2003) 490.
[18] R.B. Hill, D.P. Raleigh, A. Lombardi, W.F. Degrado, Acc. Chem. Res. 33 (2000) 745.
[19] M.L. Kennedy, B.R. Gibney, Curr. Opin. Struct. Biol. 11 (2001) 485.
[20] E.N. Salgado, R.J. Radford, F.A. Tezcan, Acc. Chem. Res. 43 (2010) 661.
[21] B.A. Shoemaker, A.R. Panchenko, PLoS Comput. Biol. 3 (2007) 595.
[22] T. Kortemme, D. Baker, Curr. Opin. Chem. Biol. 8 (2004) 91.
[23] A. Lombardi, C.M. Summa, S. Geremia, L. Randaccio, V. Pavone, W.F. DeGrado, Proc. Natl. Acad. Sci. U.S.A. 97 (2000) 6298.
[24] F.Q. Ruan, Y.Q. Chen, P.B. Hopkins, J. Am. Chem. Soc. 112 (1990) 9403.
[25] M.R. Ghadiri, C. Choi, J. Am. Chem. Soc. 112 (1990) 1630.
[26] T.M. Handel, S.A. Williams, W.F. Degrado, Science 261 (1993) 879.
[27] B.V. Popp, Z.T. Ball, J. Am. Chem. Soc. 132 (2010) 6660.
[28] R.J. Todd, R.D. Johnson, F.H. Arnold, J. Chromatogr. A 662 (1994) 13.
[29] J. Faraone-Mennella, F.A. Tezcan, H.B. Gray, J.R. Winkler, Biochemistry 45 (2006) 10504.
[30] B.A. Krantz, T.R. Sosnick, Nat. Struct. Biol. 8 (2001) 1042.
[31] E.N. Salgado, J. Faraone-Mennella, F.A. Tezcan, J. Am. Chem. Soc. 129 (2007) 13374.
[32] E.N. Salgado, R.A. Lewis, S. Mossin, A.L. Rheingold, F.A. Tezcan, Inorg. Chem. 48 (2009) 2726.
[33] E.N. Salgado, F.A. Tezcan, unpublished results.
[34] E.N. Salgado, R.A. Lewis, J. Faraone-Mennella, F.A. Tezcan, J. Am. Chem. Soc. 130 (2008) 6082.
[35] N. Froloff, A. Windemuth, B. Honig, Prot. Sci. 6 (1997) 1293.
[36] S. Kumar, R. Nussinov, Biophys. J. 83 (2002) 1595.
[37] G.I. Makhatadze, V.V. Loladze, D.N. Ermolenko, X.F. Chen, S.T. Thomas, J. Mol. Biol. 327 (2003) 1135.
[38] R. Radhakrishnan, L.J. Walter, A. Hruza, P. Reichert, P.P. Trotta, T.L. Nagabhushan, M.R. Walter, Structure 4 (1996) 1453.
[39] Z.S. Hendsch, B. Tidor, Prot. Sci. 3 (1994) 211.
[40] F.B. Sheinerman, R. Norel, B. Honig, Curr. Opin. Struct. Biol. 10 (2000) 153.
[41] M.R. Ghadiri, C. Soares, C. Choi, J. Am. Chem. Soc. 114 (1992) 825.
[42] S. Burazerovic, J. Gradinaru, J. Pierron, T.R. Ward, Angew. Chem. Int. Ed. Engl. 46 (2007) 5510.
[43] D.E. Przybyla, J. Chmielewski, J. Am. Chem. Soc. 130 (2008) 12610.
[44] Y. Lu, Curr. Opin. Chem. Biol. 9 (2005) 118.
[45] C.H.B. Chen, L. Milne, R. Landgraf, D.M. Perrin, D.S. Sigman, Chem. BioChem. 2 (2001) 735.
[46] D.F. Qi, C.M. Tann, D. Haring, M.D. DiStefano, Chem. Rev. 101 (2001) 3081.
[47] R.P. Cheng, S.L. Fisher, B. Imperiali, J. Am. Chem. Soc. 118 (1996) 11349.
[48] J.R. Carey, S.K. Ma, T.D. Pfister, D.K. Garner, H.K. Kim, J.A. Abramite, Z.L. Wang, Z.J. Guo, Y. Lu, J. Am. Chem. Soc. 126 (2004) 10812.
[49] R.J. Radford, P.C. Nguyen, T.B. Ditri, J.S. Figueroa, F.A. Tezcan, Inorg. Chem. 49 (2010) 4362.
[50] R.J. Radford, P.C. Nguyen, F.A. Tezcan, Inorg. Chem. 49 (2010) 7106.
[51] M. Brinkley, Bioconjug. Chem. 3 (1992) 2.
[52] A.E. Martell, R.M. Smith, Critical Stability Constants, Plenum Press, New York, 2010, pp. 1974–1989.
[53] H.E. Blackwell, R.H. Grubbs, Angew. Chem. Int. Ed. 37 (1998) 3281.
[54] C.E. Schafmeister, J. Po, G.L. Verdine, J. Am. Chem. Soc. 122 (2000) 5891.
[55] F.Z. Zhang, O. Sadovski, S.J. Xin, G.A. Woolley, J. Am. Chem. Soc. 129 (2007) 14154.
[56] G.L. Verdine, L.D. Walensky, Clin. Cancer Res. 13 (2007) 7264.
[57] A. Muheim, R.J. Todd, D.R. Casimiro, H.B. Gray, F.H. Arnold, J. Am. Chem. Soc. 115 (1993) 5312.
[58] R.J. Todd, M.E. Vandam, D. Casimiro, B.L. Haymore, F.H. Arnold, Proteins 10 (1991) 156.
[59] S.K. Singh, M. Trivedi, M. Chandra, A.N. Sahay, D.S. Pandey, Inorg. Chem. 43 (2004) 8600.
[60] T. Alber, Ann. Rev. Biochem. 58 (1989) 765.
[61] J.D. Klemm, S.L. Schreiber, G.R. Crabtree, Annu. Rev. Immunol. 16 (1998) 569.
[62] J.J. Kohler, S.J. Metallo, T.L. Schneider, A. Schepartz, Proc. Natl. Acad. Sci. U.S.A. 96 (1999) 11735.
[63] A. Crispini, D. Puccis, S. Sessa, A. Cataldi, A. Napoli, A. Valentini, M. Ghedini, New J. Chem. 27 (2003) 1497.
[64] T.E. Ellenberger, C.J. Brandl, K. Struhl, S.C. Harrison, Cell 71 (1992) 1223.
[65] R.V. Talanian, C.J. McKnight, P.S. Kim, Science 249 (1990) 769.
[66] B. Cuenoud, A. Schepartz, Science 259 (1993) 510.
[67] R.J. Radford, F.A. Tezcan, J. Am. Chem. Soc. 131 (2009) 9136.
[68] R.J. Radford, M. Lawrenz, P.C. Nguyen, J.A. McCammon, F.A. Tezcan, in press, doi:10.1039/C0CC02168G.
[69] E.E. Benson, A.L. Rheingold, C.P. Kubiak, Inorg. Chem. 49 (2010) 1458.
[70] T. Koshiyama, N. Kawaba, T. Hikage, M. Shirai, Y. Miura, C.Y. Huang, K. Tanaka, Y. Watanabe, T. Ueno, Bioconjug. Chem. 21 (2010) 264.
[71] Z. Huang, P.S. White, M. Brookhart, Nature 465 (2010) 598.
[72] C.Y. Yeh, C.J. Chang, D.G. Nocera, J. Am. Chem. Soc. 123 (2001) 1513.
[73] A.S. Borovik, Acc. Chem. Res. 38 (2005) 54.
[74] M.C. Thompson, D.H. Busch, J. Am. Chem. Soc. 86 (1964) 3651.
[75] I.I. Creaser, R.J. Geue, J.M. Harrowfield, A.J. Herlt, A.M. Sargeson, M.R. Snow, J. Springborg, J. Am. Chem. Soc. 104 (1982) 6016.
[76] T.J. McMurry, K.N. Raymond, P.H. Smith, Science 244 (1989) 938.
[77] J.D. Brodin, A. Medina-Morales, T. Ni, E.N. Salgado, X.I. Ambroggio, F.A. Tezcan, J. Am. Chem. Soc. 132 (2010) 8610.
[78] Y. Liu, B. Kuhlman, Nucleic Acids Res. 34 (2006) W235.
[79] X.I. Ambroggio, B. Kuhlman, J. Am. Chem. Soc. 128 (2006) 1154.
[80] A. Leaver-Fay, G.L. Butterfoss, J. Snoeyink, B. Kuhlman, J. Comput. Chem. 28 (2007) 1336.
[81] E.N. Salgado, X.I. Ambroggio, J.D. Brodin, R.A. Lewis, B. Kuhlman, F.A. Tezcan, Proc. Natl. Acad. Sci. U.S.A. 107 (2010) 1827.
[82] E.M. Nolan, J.W. Ryu, J. Jaworski, R.P. Feazell, M. Sheng, S.J. Lippard, J. Am. Chem. Soc. 128 (2006) 15517.
[83] G.K. Walkup, B. Imperiali, J. Am. Chem. Soc. 119 (1997) 3443.
[84] J.A. Hunt, M. Ahmed, C.A. Fierke, Biochemistry 38 (1999) 9054.
[85] C.E. Outten, T.V. O'Halloran, Science 292 (2001) 2488.
[86] A.C. Rosenzweig, Acc. Chem. Res. 34 (2001) 119.
[87] S. Tottey, K.J. Waldron, S.J. Firbank, B. Reale, C. Bessant, K. Sato, T.R. Cheek, J. Gray, M.J. Banfield, C. Dennison, N.J. Robinson, Nature 455 (2008) 1138.
[88] T.L. Blundell, The Evolution of Metal-Binding Sites in Proteins, Symposium Press London, University of Sussex, 1977.
[89] C.L. Liu, H.B. Xu, J. Inorg. Biochem. 88 (2002) 77.
[90] A. Volbeda, W.G.J. Hol, J. Mol. Biol. 206 (1989) 531.
[91] R.N. Armstrong, Biochemistry 39 (2000) 13625.
[92] M. Bergdoll, L.D. Eltis, A.D. Cameron, P. Dumas, J.T. Bolin, Prot. Sci. 7 (1998) 1661.
[93] N. Tokuriki, D.S. Tawfik, Science 324 (2009) 203.